Reliability Engineering and System Safety 149 (2016) 204–217

Contents lists available at ScienceDirect

Reliability Engineering and System Safety

journal homepage: www.elsevier.com/locate/ress

Model-reduction techniques for reliability-based design problems of complex structural systems

H.A. Jensen [a,*], A. Muñoz [a], C. Papadimitriou [b], E. Millas [a]

[a] Department of Civil Engineering, Santa Maria University, Valparaiso, Chile
[b] Department of Mechanical Engineering, University of Thessaly, GR-38334 Volos, Greece

ARTICLE INFO

Article history:
Received 2 July 2015
Received in revised form
29 December 2015
Accepted 1 January 2016
Available online 11 January 2016

Keywords:
Advanced simulation techniques
First excursion probability
Model reduction techniques
Reliability analysis in high dimension
Reliability-based design

ABSTRACT

This work presents a strategy for dealing with reliability-based design problems of a class of linear and nonlinear finite element models under stochastic excitation. In general, the solution of this class of problems is computationally very demanding due to the large number of finite element model analyses required during the design process. A model reduction technique combined with an appropriate optimization scheme is proposed to carry out the design process efficiently in a reduced space of generalized coordinates. In particular, a method based on component mode synthesis is implemented to define a reduced-order model for the structural system. The re-analyses of the component or substructure modes as well as the re-assembling of the reduced-order system matrices due to changes in the values of the design variables are avoided. The effectiveness of the proposed model reduction technique in the context of reliability-based design problems is demonstrated by two numerical examples.

1. Introduction

Structural design via deterministic mathematical programming techniques has been widely accepted as a viable tool for engineering design [1]. However, in most structural engineering applications response predictions are based on models involving uncertain parameters. This is due to a lack of information about the value of system parameters external to the structure such as environmental loads or internal such as system behavior. Under uncertain conditions the field of reliability-based optimization provides a realistic and rational framework for structural optimization which explicitly accounts for the uncertainties [2–4]. In the present work, structural design problems involving finite element models under stochastic loading are considered. The design problem is formulated as the minimization of an objective function subject to multiple design requirements including standard and reliability constraints. The probability that any response of interest exceeds in magnitude some specified threshold level within a given time duration is used to characterize the system reliability. This probability is commonly known as the first excursion probability [5]. The corresponding reliability problem is expressed in terms of a multidimensional probability integral involving a large number of uncertain parameters. Reliability-based design formulations require advanced and efficient tools for structural modeling, reliability analysis and mathematical programming. Modeling and analysis techniques of structural systems are well established and sufficiently well documented in the literature [6]. On the other hand, several tools for assessing structural reliability have lately experienced a substantial development providing solution of involved systems [7–9]. In the field of reliability-based optimization of stochastic dynamical systems several procedures have been recently developed allowing the solution of problems dealing with finite element models of relatively small number of degrees of freedom [10–14]. However, the application of reliability-based optimization to stochastic dynamical systems involving medium/large finite element models remains somewhat limited. In fact, the solution of reliability-based design problems of stochastic finite element models requires a large number of finite element analyses to be perform during the design process. These analyses correspond to finite element re-analyses over the design space (required by the optimizer), and system responses over the uncertain parameter space (required by the simulation technique for reliability estimation). Consequently, the computational demands depend highly on the number of finite element analyses and the time taken for performing an individual finite element analysis. Thus, the computational demands in solving reliability-based design problems may be large or even excessive.

In this context, it is the main objective of this work to present a framework for integrating a model reduction technique into the reliability-based design formulation of a class of stochastic linear and nonlinear finite element models. The goal is to reduce the time consuming operations involved in the re-analyses and

* Corresponding author.
E-mail address: hector.jensen@usm.cl (H.A. Jensen).

http://dx.doi.org/10.1016/j.ress.2016.01.003
0951-8320/

dynamic responses of medium/large finite element models. Specifically, a model reduction technique based on substructure coupling for dynamic analysis is considered in the present implementation [15]. The proposed method corresponds to a generalization of substructure coupling applicable to systems with localized nonlinearities. The technique includes dividing the linear components of the structural system into a number of substructures obtaining reduced-order models of the substructures, and then assembling a reduced-order model for the entire structure. In summary, the novel aspect of this contribution involves a strategy for integrating a model reduction technique into the reliability-based design formulation of medium/large finite element models under stochastic excitation. This represents an additional area of application of substructure coupling which has been already used for uncertainty management in structural dynamics with applications in areas such as uncertainty analysis, finite element model updating, and reliability sensitivity analysis [16–19]. The organization of this work is as follows. The formulation of the reliability-based design problem is presented in Section 2. Next, the characterization of the structural systems of interest is considered in Section 3. Implementation issues such as reliability estimation, optimization strategy and model reduction are discussed in Section 4. The mathematical background of the model reduction technique is outlined in Section 5. The integration of the model reduction technique into the design process is discussed in Section 6. The effectiveness of the proposed strategy is demonstrated in Section 7 by the reliability-based design of two structural systems. The paper closes with some conclusions and final remarks.

2. Problem formulation

The reliability-based design problem is characterized in terms of the following constrained non-linear optimization problem

$$\begin{aligned} &\text{Min}_{\boldsymbol{\theta}} \quad C(\boldsymbol{\theta}) \\ &\text{s.t.} \quad g_i(\boldsymbol{\theta}) \le 0 \qquad i = 1, \ldots, n_c \\ &\quad P_{F_i}(\boldsymbol{\theta}) - P^*_{F_i} \le 0\,, \quad i = 1, \ldots, n_r \\ &\quad \boldsymbol{\theta} \in \Theta \end{aligned} \tag{1}$$

where $\boldsymbol{\theta}, \theta_i, i = 1, \ldots, n_d$ is the vector of design variables with side constraints $\theta_i^l \le \theta_i \le \theta_i^u$, $C(\boldsymbol{\theta})$ is the objective function, $g_i(\boldsymbol{\theta}) \le 0, i = 1, \ldots, n_c$ are standard constraints, and $P_{F_i}(\boldsymbol{\theta}) - P^*_{F_i} \le 0$ are the reliability constraints which are defined in terms of the failure probability functions $P_{F_i}(\boldsymbol{\theta})$ and target failure probabilities $P^*_{F_i}$, $i = 1, \ldots, n_r$. It is assumed that the objective and constraint functions are smooth functions of the design variables. The objective function $C(\boldsymbol{\theta})$ can be defined in terms of initial, construction, repair or downtime costs, structural weight, or general cost functions. The standard constraints are related to general design requirements such as geometric conditions, material cost components, and availability of materials. On the other hand, the reliability constraints are associated with design specifications characterized through the use of reliability measures given in terms of failure probabilities with respect to specific failure criteria. For structural systems under stochastic excitation the probability that design conditions are satisfied within a particular reference period T provides a useful reliability measure [5]. Such measure is referred as the first excursion probability and quantifies the plausibility of the occurrence of unacceptable behavior (failure) of the structural system. In this context, a failure event F_i can be defined as $F_i(\boldsymbol{\theta}, \mathbf{z}) = d_i(\boldsymbol{\theta}, \mathbf{z}) > 1$, where d_i is the so-called normalized demand function defined as $d_i(\boldsymbol{\theta}, \mathbf{z}) = \max_{j=1,\ldots,l} \max_{t \in [0,T]} |r_j^i(t, \boldsymbol{\theta}, \mathbf{z})| / r_j^{i^*}$, where $\mathbf{z} \in \Omega_{\mathbf{z}} \subset R^{n_z}$ is the vector of uncertain variables involved in the problem (characterization of the excitation), $r_j^i(t, \boldsymbol{\theta}, \mathbf{z}), j = 1, \ldots, l$ are the response functions associated with the failure event F_i, and $r_j^{i^*}$ is the acceptable response level for the response r_j^i. It is clear that the responses $r_j^i(t, \boldsymbol{\theta}, \mathbf{z})$ are functions of time (due to the dynamic nature of the excitation), the design vector $\boldsymbol{\theta}$, and the random vector $\mathbf{z}$. These response functions are obtained from the solution of the equation of motion that characterizes the structural model (see next Section). The uncertain variables $\mathbf{z}$ are modeled using a prescribed probability density function $p(\mathbf{z})$. This function indicates the relative plausibility of the possible values of the uncertain parameters $\mathbf{z} \in \Omega_{\mathbf{z}}$. The probability of failure evaluated at the design $\boldsymbol{\theta}$ is formally defined as

$$P_{F_i}(\boldsymbol{\theta}) = P\left[\max_{j=1,\ldots,l} \max_{t \in [0,T]} \frac{|r_j^i(t, \boldsymbol{\theta}, \mathbf{z})|}{r_j^{i^*}} > 1\right] \tag{2}$$

where $P[\cdot]$ is the probability that the expression in parenthesis is true. Equivalently, the failure probability function evaluated at the design $\boldsymbol{\theta}$ can be written in terms of the multidimensional probability integral

$$P_{F_i}(\boldsymbol{\theta}) = \int_{d_i(\boldsymbol{\theta}, \mathbf{z}) > 1} p(\mathbf{z})\, d\mathbf{z} \tag{3}$$

It is noted that the above formulation can be extended in a direct manner if the cost of partial or total failure consequences is also included in the definition of the objective function. It is also noted that constraints related to statistics of structural responses (i.e. mean value and/or higher-order statistical moments) can be included in the formulation as well. Thus, the above formulation is quite general in the sense that different reliability-based optimization formulations can be considered.

3. Mechanical modeling

A quite general class of structural dynamical systems can be cast into the following equation of motion

$$\mathbf{M}\ddot{\mathbf{u}}(t) + \mathbf{C}\dot{\mathbf{u}}(t) + \mathbf{K}\mathbf{u}(t) = \mathbf{k}(\mathbf{u}(t), \dot{\mathbf{u}}(t), \boldsymbol{\tau}(t)) + \mathbf{f}(t) \tag{4}$$

where $\mathbf{u}(t)$ denotes the displacement vector of dimension n, $\dot{\mathbf{u}}(t)$ the velocity vector, $\ddot{\mathbf{u}}(t)$ the acceleration vector, $\mathbf{k}(\mathbf{u}(t), \dot{\mathbf{u}}(t), \boldsymbol{\tau}(t))$ the vector of non-linear restoring forces, $\boldsymbol{\tau}(t)$ the vector of a set of variables which describes the state of the nonlinear components, and $\mathbf{f}(t)$ the external force vector. The matrices $\mathbf{M}$, $\mathbf{C}$, and $\mathbf{K}$ describe the mass, damping, and stiffness, respectively. Note that some of the matrices and vectors involved in the equation of motion depend on the vector of design variables $\boldsymbol{\theta}$ and/or the uncertain system parameters $\mathbf{z}$ and therefore the solution is also a function of these quantities. The explicit dependence of the response on these quantities is not shown here for simplicity in notation. The evolution of the set of variables $\boldsymbol{\tau}(t)$ is described by a first-order differential equation

$$\dot{\boldsymbol{\tau}}(t) = \boldsymbol{\kappa}(\mathbf{u}(t), \dot{\mathbf{u}}(t), \boldsymbol{\tau}(t)) \tag{5}$$

where $\boldsymbol{\kappa}$ represents a non-linear vector function. This characterization allows to model different types of nonlinearities including hysteresis and degradation [20,21]. From Eq. (5) it is seen that the set of variables $\boldsymbol{\tau}(t)$ is a function of the displacements $\mathbf{u}(t)$ and the velocities $\dot{\mathbf{u}}(t)$, i.e. $\boldsymbol{\tau}(\mathbf{u}(t), \dot{\mathbf{u}}(t))$. Therefore, Eqs. (4) and (5) constitute a system of coupled non-linear differential equations for $\mathbf{u}(t)$ and $\boldsymbol{\tau}(t)$. The previous formulation is particularly well suited for cases where most of the components of the structural system remain linear and only a small part behaves in a nonlinear manner. Such cases are of particular interest in the present work, that is, linear finite element models with localized nonlinearities. The external force vector $\mathbf{f}(t)$ is modeled as a non-stationary stochastic process. Depending on the application under consideration different methodologies are available for generating these types of processes. Such methodologies include filtered Gaussian white noise processes, stochastic processes compatible with power spectral densities, point source-based models, and record-based

models [5,22–25]. A common aspect of the aforementioned methodologies is that the generation of the corresponding stochastic processes samples involves in general a large number of random variables, e.g. of the order of hundreds or thousands. Therefore, the evaluation of the reliability constraints for a given design constitutes a high-dimensional problem which is extremely demanding from a numerical point of view.

4. Implementation issues

4.1. Reliability estimation

The reliability constraints of the nonlinear constrained optimization problem (1) are defined in terms of the first excursion probability functions $P_{F_i}(\boldsymbol{\theta})$, $i=1,\ldots n_r$. As previously pointed out, these reliability measures are given in terms of high-dimensional integrals. The difficulty in estimating these quantities favors the application of simulation techniques to cope with the probability integrals [26]. It is important to note that each sample implies the solution of the equation of motion that characterizes the structural model (a dynamic finite element model analysis). Therefore an efficient simulation technique is required in the context of the present formulation. A general applicable method named subset simulation is adopted here [7]. In this well known advanced simulation technique the failure probabilities are expressed as a product of conditional probabilities of some chosen intermediate failure events, the evaluation of which only requires simulation of more frequent events. The intermediate failure events are chosen adaptively using information from simulated samples so that they correspond to some specified values of conditional failure probabilities. Therefore, a rare event simulation problem is converted into a sequence of more frequent event simulation problems. The method uses a Markov chain Monte Carlo method based on the Metropolis algorithm for sampling from the conditional probabilities [27]. This is the most widely applicable simulation technique because it is not based on any geometrical assumption about the topology of the failure domain. In fact, validation calculations have shown that subset simulation can be applied efficiently to a wide range of dynamical systems including general linear and non-linear systems [28,29]. In addition, subset simulation is very-well suited for parallel implementation in a computer cluster [30]. For a detailed description and numerical implementation of subset simulation see references [7,29,31].

4.2. Optimization strategy

The solution of the reliability-based optimization problem defined in Eq. (1) can be obtained in principle by a number of techniques such as standard deterministic optimization schemes or stochastic search algorithms [1,12,32]. In particular, a class of interior point algorithms based on the solution of the first-order optimality conditions is considered for solving the numerical examples presented in this work [33]. In general, the above scheme has proved to be quite effective for a wide range of applications in the context of deterministic and stochastic optimization problems [34,35]. Since the focus of this work is not on the optimization strategy but on the integration of a model reduction technique into the reliability-based design formulation of medium/large stochastic finite element models, the reader is referred to [33,35] for a detailed description and implementation of the aforementioned algorithm.

4.3. Model reduction

The solution of the reliability-based optimization problem (1) is computationally very demanding due to the large number of dynamic analyses required during the design process. In fact the reliability estimation at each design requires the evaluation of the system response at a large number of samples in the uncertain parameter space (of the order of hundreds or thousands). In addition, the iterative nature of the optimization strategy may impose additional computational demands. Consequently, the computational cost may become excessive when the computational time for performing a dynamic analysis is significant. To cope with this difficulty, a model reduction technique is considered in the present formulation. In particular, a method based on substructure coupling or component-mode synthesis is implemented in order to define a reduced-order model for the structural system [15,17]. The general idea is to divide the linear components of the structural system into a number of linear substructures obtaining reduced-order models and then assembling a reduced-order model of the entire structural system.

4.4. Synopsis of proposed methodology

The mathematical background of the model reduction technique and its integration into the design process are discussed in Sections 5 and 6. In Section 5 the transformation matrix that define the set of generalized coordinates of the reduced-order model is first defined. Based on the new set of coordinates the reduced-order model matrices are derived. Then, the response of the system in terms of the reduced-order model is discussed. Next, the design process based on the reduced-order model is outlined in Section 6. First, a particular finite element model parametrization scheme that allows to represent the substructure matrices explicitly in terms of the design variables is introduced. The representation of the substructure matrices is then used to construct an expansion of the reduced-order model matrices with respect to the design variables. Based on this expansion it is demonstrated that the reduced-order model matrices need to be computed and assembled once during the entire design process. This in turn implies a drastic reduction in the computational demands involved in the design of complex structural systems. Finally, some advantages and limitations of the proposed formulation are discussed.

5. Component mode synthesis technique

5.1. Substructure modes

In the present formulation fixed-interface normal modes and interface constraint modes are considered in order to define the reduced-order model [15]. To this end, the following partitioned form of the mass matrix $\mathbf{M}^s \in R^{n^s \times n^s}$ and stiffness matrix $\mathbf{K}^s \in R^{n^s \times n^s}$ of the substructure $s, s=1,\ldots,N_s$, is considered

$$\mathbf{M}^s = \begin{bmatrix} \mathbf{M}^s_{ii} & \mathbf{M}^s_{ib} \\ \mathbf{M}^s_{bi} & \mathbf{M}^s_{bb} \end{bmatrix}, \quad \mathbf{K}^s = \begin{bmatrix} \mathbf{K}^s_{ii} & \mathbf{K}^s_{ib} \\ \mathbf{K}^s_{bi} & \mathbf{K}^s_{bb} \end{bmatrix} \tag{6}$$

where the indices i and b are sets containing the internal and boundary degrees of freedom of the substructure s, respectively. The boundary degrees of freedom include only those that are common with the boundary degrees of freedom of adjacent substructures, while the internal degrees of freedom are not shared with any adjacent substructure. In this framework, all boundary coordinates are kept as one set $\mathbf{u}^s_b(t) \in R^{n^s_b}$ and the internal coordinates in the set $\mathbf{u}^s_i(t) \in R^{n^s_i}$. The displacement vector of physical

coordinates of the substructure s is given by $\mathbf{u}^s(t)^T = \langle \mathbf{u}_i^s(t)^T, \mathbf{u}_b^s(t)^T \rangle \in R^{n^s}$ where $n^s = n_i^s + n_b^s$, and the symbol $\langle\ \rangle$ represents a row vector. The fixed-interface normal modes are obtained by restraining all boundary degrees of freedom and solving the eigenproblem

$$\mathbf{K}_{ii}^s \boldsymbol{\Phi}_{ii}^s - \mathbf{M}_{ii}^s \boldsymbol{\Phi}_{ii}^s \boldsymbol{\Lambda}_{ii}^s = \mathbf{0} \tag{7}$$

where the matrix $\boldsymbol{\Phi}_{ii}^s$ contains the complete set of $n_i{}^s$ fixed-interface normal modes, and $\boldsymbol{\Lambda}_{ii}^s$ is the corresponding matrix containing the eigenvalues. The fixed-interface normal modes are normalized with respect to the mass matrix $\mathbf{M}_{ii}^s$ satisfying $\boldsymbol{\Phi}_{ii}^{sT} \mathbf{M}_{ii}^s \boldsymbol{\Phi}_{ii}^s = \mathbf{I}_{ii}^s$, and $\boldsymbol{\Phi}_{ii}^{sT} \mathbf{K}_{ii}^s \boldsymbol{\Phi}_{ii}^s = \boldsymbol{\Lambda}_{ii}^s$. On the other hand, the interface constraint modes are defined by setting a unit displacement on the boundary coordinates $\mathbf{u}_b^s(t)$ and zero forces in the internal degrees of freedom. Then, the set of interface constraint modes is given by

$$\begin{bmatrix} \mathbf{K}_{ii}^s & \mathbf{K}_{ib}^s \\ \mathbf{K}_{bi}^s & \mathbf{K}_{bb}^s \end{bmatrix} \begin{bmatrix} \boldsymbol{\Psi}_{ib}^s \\ \mathbf{I}_{bb}^s \end{bmatrix} = \begin{bmatrix} \mathbf{0}_{ib}^s \\ \mathbf{R}_{bb}^s \end{bmatrix} \tag{8}$$

from where the interface constraint-mode matrix $\boldsymbol{\Psi}_c^s$ can be defined as

$$\boldsymbol{\Psi}_c^s = \begin{bmatrix} \boldsymbol{\Psi}_{ib}^s \\ \mathbf{I}_{bb}^s \end{bmatrix} = \begin{bmatrix} -\mathbf{K}_{ii}^{s\,-1} \mathbf{K}_{ib}^s \\ \mathbf{I}_{bb}^s \end{bmatrix} \tag{9}$$

where $\boldsymbol{\Psi}_{ib}^s \in R^{n_i^s \times n_b^s}$ is the interior partition of the interface constraint-mode matrix.

5.2. Reduced-order model

Based on the previous fixed-interface normal modes and interface constraint modes a displacement transformation matrix is introduced to define a set of generalized coordinates. Such transformation corresponds to the Craig–Bampton method [15], and it takes the form:

$$\mathbf{u}^s(t) = \begin{Bmatrix} \mathbf{u}_i^s(t) \\ \mathbf{u}_b^s(t) \end{Bmatrix} = \begin{bmatrix} \boldsymbol{\Phi}_{ik}^s & \boldsymbol{\Psi}_{ib}^s \\ \mathbf{0}_{bk}^s & \mathbf{I}_{bb}^s \end{bmatrix} \begin{Bmatrix} \mathbf{v}_k^s(t) \\ \mathbf{v}_b^s(t) \end{Bmatrix} = \boldsymbol{\Psi}^s \quad \mathbf{v}^s(t) \tag{10}$$

where $\boldsymbol{\Phi}_{ik}^s \in R^{n_i^s \times n_k^s}$ is the interior partition of the matrix $\boldsymbol{\Phi}_{ii}^s$ of the $n_k{}^s$ kept fixed-interface normal modes, $\mathbf{v}^s(t)$ represents the substructure generalized coordinates composed by the modal coordinates $\mathbf{v}_k^s(t)$ of the kept fixed-interface normal modes and the boundary coordinates $\mathbf{v}_b^s(t) = \mathbf{u}_b^s(t)$, $\boldsymbol{\Psi}^s \in R^{n^s \times \hat{n}^s}$ is the Craig–Bampton transformation matrix with $\hat{n}^s = n_k^s + n_b^s$, and all other terms have been previously defined. The substructure mass matrix $\hat{\mathbf{M}}^s \in R^{\hat{n}^s \times \hat{n}^s}$ and stiffness matrix $\hat{\mathbf{K}}^s \in R^{\hat{n}^s \times \hat{n}^s}$ in generalized coordinates $\mathbf{v}^s(t)$ are given by

$$\hat{\mathbf{M}}^s = \boldsymbol{\Psi}^{sT} \mathbf{M}^s \boldsymbol{\Psi}^s, \quad \hat{\mathbf{K}}^s = \boldsymbol{\Psi}^{sT} \mathbf{K}^s \boldsymbol{\Psi}^s \tag{11}$$

Next, the vector of generalized coordinates for all the N_s substructures

$$\mathbf{v}(t)^T = \langle \mathbf{v}^1(t)^T, \ldots, \mathbf{v}^{N_s}(t)^T \rangle \in R^{n_v} \tag{12}$$

where $n_v = \sum_{s=1}^{N_s} \hat{n}^s$ is introduced. Based on this vector, a new vector $\mathbf{q}(t)$ that contains the independent generalized coordinates consisting of the fixed-interface modal coordinates $\mathbf{v}_k^s(t)$ for each substructure and the physical coordinates $\mathbf{v}_b^l(t)$, $l = 1, \ldots, N_b$ at the N_b interfaces is defined as

$$\mathbf{q}(t)^T = \langle \mathbf{v}_k^1(t)^T, \ldots, \mathbf{v}_k^{N_s}(t)^T, \mathbf{v}_b^1(t)^T, \ldots, \mathbf{v}_b^{N_b}(t)^T \rangle \in R^{n_q} \tag{13}$$

where $n_q = \sum_{s=1}^{N_s} n_k^s + \sum_{l=1}^{N_b} n_b^l$, and $n_b{}^l$ is the number of degrees of freedom at the interface l ($l = 1, \ldots, N_b$). These two vectors are related by the transformation:

$$\mathbf{v}(t) = \mathbf{T}\mathbf{q}(t) \tag{14}$$

where the matrix $\mathbf{T} \in R^{n_v \times n_q}$ is a matrix of zeros and ones that couples the independent generalized coordinates $\mathbf{q}(t)$ of the reduced system with the generalized coordinates of each substructure. The assembled mass matrix $\hat{\mathbf{M}} \in R^{n_q \times n_q}$ and the stiffness matrix $\hat{\mathbf{K}} \in R^{n_q \times n_q}$ for the independent reduced set $\mathbf{q}(t)$ of generalized coordinates take the form:

$$\hat{\mathbf{M}} = \mathbf{T}^T \begin{bmatrix} \hat{\mathbf{M}}^1 & \mathbf{0} & \mathbf{0} \\ \mathbf{0} & \ddots & \mathbf{0} \\ \mathbf{0} & \mathbf{0} & \hat{\mathbf{M}}^{N_s} \end{bmatrix} \mathbf{T}, \quad \hat{\mathbf{K}} = \mathbf{T}^T \begin{bmatrix} \hat{\mathbf{K}}^1 & \mathbf{0} & \mathbf{0} \\ \mathbf{0} & \ddots & \mathbf{0} \\ \mathbf{0} & \mathbf{0} & \hat{\mathbf{K}}^{N_s} \end{bmatrix} \mathbf{T} \tag{15}$$

The number of fixed-interface normal modes to be used in the reduced-order model can be established by using different criteria. One particular criterion is discussed in the Numerical Examples Section. Finally, it is also noted that further reduction in the generalized coordinates can be achieved by replacing the interface degrees of freedom by a reduced number of interface modes. That is, the displacement coordinates $\mathbf{v}_b^l(t) \in R^{n_b^l}$ at the interface l can be expressed in terms of a set of generalized coordinates [17]. For simplicity and clarity all interface degrees of freedom are kept in the present implementation.

5.3. Reduced-order model response

In order to write the equation of motion of the structural system in terms of the reduced set of generalized coordinates $\mathbf{q}(t)$, it is first observed that the independent physical coordinates $\mathbf{u}(t)$ of the original unreduced structural model can be written directly in terms of $\mathbf{q}(t)$ as

$$\mathbf{u}(t) = \overline{\mathbf{T}} \boldsymbol{\Psi} \mathbf{T} \mathbf{q}(t) \tag{16}$$

where $\overline{\mathbf{T}} \in R^{n \times n_u}$ is a constant matrix that map the vector $\overline{\mathbf{u}}(t)^T = < \mathbf{u}^1(t)^T, \ldots, \mathbf{u}^{N_s}(t)^T > \in R^{n_u}, n_u = \sum_{s=1}^{N_s} n^s$ of the physical coordinates of all substructures to $\mathbf{u}(t)$, and $\boldsymbol{\Psi} \in R^{n_u \times n_v}$ is a block diagonal matrix defined in terms of the Craig–Bampton transformation matrices of all substructures, that is, $\boldsymbol{\Psi} = blockdiag(\boldsymbol{\Psi}^1, \ldots, \boldsymbol{\Psi}^{N_s})$. Based on this transformation, the equation of motion of the reduced-order system can be written as

$$\hat{\mathbf{M}}\ddot{\mathbf{q}}(t) + \hat{\mathbf{C}}\dot{\mathbf{q}}(t) + \hat{\mathbf{K}}\mathbf{q}(t) = \mathbf{T}^T \boldsymbol{\Psi}^T \overline{\mathbf{T}}^T \mathbf{k}(\mathbf{u}(t), \dot{\mathbf{u}}(t), \boldsymbol{\tau}(t)) + \mathbf{T}^T \boldsymbol{\Psi}^T \overline{\mathbf{T}}^T \mathbf{f}(t) \tag{17}$$

where $\hat{\mathbf{C}} \in R^{n_q \times n_q}$ is the assembled damping matrix for the independent reduced set $\mathbf{q}(t)$, which can be defined in terms of the substructures damping matrices in generalized coordinates $\mathbf{v}^s(t)$ as $\hat{\mathbf{C}}^s = \boldsymbol{\Psi}^{sT} \mathbf{C}^s \boldsymbol{\Psi}^s$, $s = 1, \ldots, N_s$, and all other terms have been previously defined. The assembled damping matrix has a similar structure as $\hat{\mathbf{M}}$ and $\hat{\mathbf{K}}$ (see Eq. (15)). It is noted that the dimension of the matrices involved in the equation of motion of the reduced-order model can be substantially smaller than the dimension of the unreduced matrices, e.g. $n_q \ll n$. It is also noted that the vector of non-linear restoring forces can be characterized in local component specific coordinates, due to the localized non-linearities, with a minimal number of variables. These local variables are related to the vector of independent physical coordinates $\mathbf{u}(t)$ by a standard linear transformation matrix. In this manner, the set of nonlinear Eqs. (5) and (17) can be integrated efficiently by an appropriate step-by-step integration scheme [6] or by modal analysis [19,36,37]. Finally, it should be pointed out that the matrices involved in the equation of motion of the original system may depend on the vector of design variables $\boldsymbol{\theta}$, and therefore a number of the quantities that appear in this section are also function of $\boldsymbol{\theta}$. The explicit dependence of those quantities on $\boldsymbol{\theta}$ is examined in the following section.

6. Design based on the reduced-order model

The previous model reduction technique is quite general in the sense that dividing the structure into substructures and reducing

the number of physical coordinates to a much smaller number of generalized coordinates certainly alleviates part of the computational effort. However, the generation of the reduced-order model at each design implies the solution of the fixed-interface normal modes eigenproblem and the computation of the interface constraint modes for each substructure. This procedure can be computationally very expensive due to the substantial computational overhead that arises at substructure level. In order to make the model reduction technique more efficient a particular parametrization scheme in terms of the design variables is considered in the present formulation. Specifically, it is assumed that the stiffness and mass matrix of a substructure $s, s=1,\ldots,N_s$, depend on only one of the design variables. Such dependency can be linear or nonlinear. Clearly, the case in which the stiffness and mass matrix of a substructure s do not depend on the design variables is also included in this parametrization scheme. It should be pointed out that the previous parametrization is often encountered in a number of practical applications [17,19]. The analysis of the reduced-order model based on this particular parametrization scheme is presented in this section. Some remarks regarding the more general case for which the stiffness and mass matrices of a substructure depend on more than one design variable are provided at the end of the section.

6.1. Normal and constraint modes

Let S_0 be the set of substructures that do not depend on the vector of design variables $\boldsymbol{\theta}$. In this case the substructure stiffness and mass matrices are written as $\mathbf{K}^s=\mathbf{K}_0^s$ and $\mathbf{M}^s=\mathbf{M}_0^s$. The substructure fixed-interface normal modes and interface constraint modes are independent of the design variables value. Thus, only a single analysis is required to estimate the interface modes for the particular substructure s. The substructure modes of these substructures are computed once during the design process. In other words, the eigenvalue problem to compute the eigenvalues and mode shapes of the kept fixed-interface normal modes $\boldsymbol{\Phi}_{ik}^s$ as well as the solution of the linear system to compute the interface constraint modes $\boldsymbol{\Psi}_{ib}^s$ for a component $s\in S_0$ are not repeated at each iteration of the design process.

On the other hand, let S_j be the set of substructures that depend on the design variable θ_j. It is assumed that the stiffness and mass matrices take the general form

$$\mathbf{K}^s=\overline{\mathbf{K}}^s h^j(\theta_j),\quad \mathbf{M}^s=\overline{\mathbf{M}}^s g^j(\theta_j) \tag{18}$$

where the reference matrices $\overline{\mathbf{K}}^s$ and $\overline{\mathbf{M}}^s$ are independent of θ_j, and $h^j(\theta_j)$ and $g^j(\theta_j)$ are linear or nonlinear functions of the design variable θ_j. It is clear that the partitions of the stiffness matrix $\mathbf{K}^s$ and mass matrix $\mathbf{M}^s$ (see Eq. (6)) admit the same parametrization. Then, the eigenvalues and eigenvectors associated with the kept fixed-interface normal modes can be expressed as

$$\boldsymbol{\Lambda}_{kk}^s=\overline{\boldsymbol{\Lambda}}_{kk}^s\frac{h^j(\theta_j)}{g^j(\theta_j)},\quad \boldsymbol{\Phi}_{ik}^s=\overline{\boldsymbol{\Phi}}_{ik}^s\frac{1}{\sqrt{g^j(\theta_j)}} \tag{19}$$

where the matrices $\overline{\boldsymbol{\Lambda}}_{kk}^s$ and $\overline{\boldsymbol{\Phi}}_{ik}^s$ are the solution of the eigenproblem

$$\overline{\mathbf{K}}_{ii}^s\overline{\boldsymbol{\Phi}}_{ik}^s-\overline{\mathbf{M}}_{ii}^s\overline{\boldsymbol{\Phi}}_{ik}^s\overline{\boldsymbol{\Lambda}}_{kk}^s=\mathbf{0} \tag{20}$$

where the matrices $\overline{\boldsymbol{\Phi}}_{ik}^s$ and $\overline{\boldsymbol{\Lambda}}_{kk}^s$ of the reference eigenvectors and eigenvalues, respectively, are independent of θ_j. Since the fixed-interface normal mode are normalized with respect to the mass matrix $\mathbf{M}_{ii}^s$ (see Section 5.1), it is easily shown that the reference mode shapes $\overline{\boldsymbol{\Phi}}_{ik}^s$ satisfy the orthogonal conditions $\overline{\boldsymbol{\Phi}}_{ik}^{sT}\overline{\mathbf{M}}_{ii}^s\overline{\boldsymbol{\Phi}}_{ik}^s=\mathbf{I}_{kk}^s$, and $\overline{\boldsymbol{\Phi}}_{ik}^{sT}\overline{\mathbf{K}}_{ii}^s\overline{\boldsymbol{\Phi}}_{ik}^s=\overline{\boldsymbol{\Lambda}}_{kk}^s$. Furthermore, the interface constraint modes are also independent of θ_j since

$$\boldsymbol{\Psi}_{ib}^s=-\mathbf{K}_{ii}^{s\,-1}\mathbf{K}_{ib}^s=-\overline{K}_{ii}^{s\,-1}\,h^{j\,-1}(\theta_j)\overline{\mathbf{K}}_{ib}^s\,h^j(\theta_j)=-\overline{\mathbf{K}}_{ii}^{s\,-1}\overline{\mathbf{K}}_{ib}^s=\overline{\boldsymbol{\Psi}}_{ib}^s \tag{21}$$

Using (Eqs. (19) and (20)), a single eigen-analysis of each substructure is required to provide the exact estimate of the normal and constraint modes for any value of the design variable θ_j. This is a very important result in the context of the proposed formulation since the computationally intensive re-analyses for estimating the fixed-interface constrained modes and the interface constraint modes of each substructure for different values of θ_j required during the design process are completely avoided. In addition, the previous result allows to express the reduced-order model matrices explicitly in terms of the design variables (see next sections). This in turn has a significant implication in terms of the computational efforts involved during the design process (see Section 7). Finally, it is emphasized that the restriction regarding the matrices dependence on one design variable is at substructure level. Of course different substructures can depend on different design variables.

6.2. Substructure matrices

The substructure mass matrix $\hat{\mathbf{M}}^s\in R^{\hat{n}^s\times\hat{n}^s}$ and stiffness matrix $\hat{\mathbf{K}}^s\in R^{\hat{n}^s\times\hat{n}^s}$ in generalized coordinates $\mathbf{v}^s(t)$ are given in Eq. (11). Based on the previous parametrization, it can be shown that the partitions for the substructure stiffness matrices $\hat{\mathbf{K}}_{kk}^s\in R^{n_k^s\times n_k^s}$, $\hat{\mathbf{K}}_{kb}^s\in R^{n_k^s\times n_b^s}$, $\hat{\mathbf{K}}_{bb}^s\in R^{n_b^s\times n_b^s}$ and mass matrices $\hat{\mathbf{M}}_{kk}^s\in R^{n_k^s\times n_k^s}$, $\hat{\mathbf{M}}_{kb}^s\in R^{n_k^s\times n_b^s}$ $\hat{\mathbf{M}}_{bb}^s\in R^{n_b^s\times n_b^s}$ of a substructure $s\in S_j$ follow the parametrization

$$\hat{\mathbf{K}}_{kk}^s=\overline{\boldsymbol{\Lambda}}_{kk}^s\frac{h^j(\theta_j)}{g^j(\theta_j)},\quad \hat{\mathbf{K}}_{kb}^s=\hat{\mathbf{K}}_{bk}^{sT}=\mathbf{0}_{kb}^s,\quad \hat{\mathbf{K}}_{bb}^s=(\overline{\mathbf{K}}_{bb}^s+\overline{\mathbf{K}}_{bi}^s\overline{\boldsymbol{\Psi}}_{ib}^s)h^j(\theta_j) \tag{22}$$

and

$$\hat{\mathbf{M}}_{kk}^s=\mathbf{I}_{kk},\quad \hat{\mathbf{M}}_{kb}^s=\hat{\mathbf{M}}_{bk}^{sT}=(\overline{\boldsymbol{\Phi}}_{ik}^{sT}\overline{\mathbf{M}}_{ii}^s\overline{\boldsymbol{\Psi}}_{ib}^s+\overline{\boldsymbol{\Phi}}_{ik}^{sT}\overline{\mathbf{M}}_{ib}^s)\sqrt{g^j(\theta_j)}$$

$$\hat{\mathbf{M}}_{bb}^s=[(\overline{\boldsymbol{\Psi}}_{ib}^{sT}\overline{\mathbf{M}}_{ii}^s+\overline{\mathbf{M}}_{bi}^s)\overline{\boldsymbol{\Psi}}_{ib}^s+\overline{\boldsymbol{\Psi}}_{ib}^{sT}\overline{\mathbf{M}}_{ib}^s+\overline{\mathbf{M}}_{bb}^s]g^j(\theta_j) \tag{23}$$

The partitions in Eqs. (22) and (23) have been derived from (11) using the form of $\boldsymbol{\Psi}^s$ defined in (10), after substituting the matrices $\boldsymbol{\Phi}_{ik}^s$, $\boldsymbol{\Lambda}_{kk}^s$, and $\boldsymbol{\Psi}_{ib}^s$ from the expressions (19) and (21).

6.3. Parametrization of reduced-order matrices

Substituting into Eq. (15) the previous characterization of the substructure matrices partitions, the stiffness matrix of the reduced-order system can be written as

$$\hat{\mathbf{K}}=\hat{\mathbf{K}}_0+\sum_{j=1}^{n_d}\left\{\hat{\overline{\mathbf{K}}}_{1j}\frac{h^j(\theta_j)}{g^j(\theta_j)}+\hat{\overline{\mathbf{K}}}_{2j}h^j(\theta_j)\right\} \tag{24}$$

where n_d is the number of independent design variables, and the matrices $\hat{\mathbf{K}}_0$, $\hat{\overline{\mathbf{K}}}_{1j}$ and $\hat{\overline{\mathbf{K}}}_{2j}$, $j=1,\ldots,n_d$ are constant matrices. Similarly, the mass matrix of the reduced-order system can be characterized as

$$\hat{\mathbf{M}}=\hat{\mathbf{M}}_0+\sum_{j=1}^{n_d}\{\hat{\overline{\mathbf{M}}}_{1j}+\hat{\overline{\mathbf{M}}}_{2j}\sqrt{g^j(\theta_j)}+\hat{\overline{\mathbf{M}}}_{3j}g^j(\theta_j)\} \tag{25}$$

where the matrices $\hat{\mathbf{M}}_0$, $\hat{\overline{\mathbf{M}}}_{1j}$, $\hat{\overline{\mathbf{M}}}_{2j}$, and $\hat{\overline{\mathbf{M}}}_{3j}$, $j=1,\ldots,n_d$ are also constant matrices. The definition of the above matrices is provided

in Appendix A. It is important to emphasize that the assembled matrices $\hat{\mathbf{K}}_0$, $\hat{\mathbf{K}}_{1j}$, $\hat{\mathbf{K}}_{2j}$, $\hat{\mathbf{M}}_0$, $\hat{\mathbf{M}}_{1j}$, $\hat{\mathbf{M}}_{2j}$ and $\hat{\mathbf{M}}_{3j}$ in the expansions (24) and (25) are independent of the values of the vector of design variables $\boldsymbol{\theta}$. To save computational time these matrices are computed and assembled once for a reference model obtained from the original model by setting $h^j(\theta_j)=1$, and $g^j(\theta_j)=1$. Therefore there is no need for this computation to be repeated during the iterations of the design process due to the changes in value of the design variables. This feature results in substantial computational savings since it avoids re-computing the fixed-interface and constraint modes for each substructure and also avoids assembling the reduced matrices from these substructures. The formulation guarantees that the reduced model is based on the exact substructure modes for all values of the design variables. In summary, the reduced-order substructure matrices are computed once during the design process.

6.4. Parametrization of global transformation matrix

Finally, it is noted that the transformation matrix $\overline{\mathbf{T}}\boldsymbol{\Psi}\mathbf{T}$ that relates the independent physical coordinates $\mathbf{u}(t)$ with the generalized coordinates of the reduced-order model $\mathbf{q}(t)$ (see Eqs. (16) and (17)) can also be written explicitly in terms of the design variables. In fact, using the structure of $\boldsymbol{\Psi}^s$ and the dependence of $\boldsymbol{\Phi}^s_{ik}$ and $\boldsymbol{\Psi}^s_{ib}$ on θ_j derived in (19) and (21) respectively, this transformation matrix can be expressed as

$$\begin{aligned}\overline{\mathbf{T}}\boldsymbol{\Psi}\mathbf{T} &= \overline{\mathbf{T}}\ blockdiag\ (\overline{\boldsymbol{\Psi}}^1\delta_{10},\ldots,\overline{\boldsymbol{\Psi}}^{N_s}\delta_{N_s0})\mathbf{T}\\ &+\sum_{j=1}^{n_d}[\overline{\mathbf{T}}\ blockdiag\ (\overline{\boldsymbol{\Psi}}^1_1\delta_{1j},\ldots,\overline{\boldsymbol{\Psi}}^{N_s}_1\delta_{N_sj})\mathbf{T}\frac{1}{\sqrt{g^j(\theta_j)}}\\ &+\overline{\mathbf{T}}\ blockdiag\ (\overline{\boldsymbol{\Psi}}^1_2\delta_{1j},\ldots,\overline{\boldsymbol{\Psi}}^{N_s}_2\delta_{N_sj})\mathbf{T}]\end{aligned} \tag{26}$$

where $\overline{\boldsymbol{\Psi}}^s$ is the Craig–Brampton transformation matrix of a substructure s that does not depend on the design variables, $\overline{\boldsymbol{\Psi}}^s_1$ and $\overline{\boldsymbol{\Psi}}^s_2$ are matrices associated with the Craig–Brampton transformation matrix of a substructure s that depends on the design variable θ_j, with

$$\overline{\boldsymbol{\Psi}}^s_1=\begin{bmatrix}\overline{\boldsymbol{\Phi}}^s_{ik} & \mathbf{0}^s_{ib}\\ \mathbf{0}^s_{bk} & \mathbf{0}^s_{bb}\end{bmatrix},\quad \overline{\boldsymbol{\Psi}}^s_2=\begin{bmatrix}\mathbf{0}^s_{ik} & \overline{\boldsymbol{\Psi}}^s_{ib}\\ \mathbf{0}^s_{bk} & \mathbf{I}^s_{bb}\end{bmatrix} \tag{27}$$

Note that the matrices $\overline{\boldsymbol{\Psi}}^s_1$ and $\overline{\boldsymbol{\Psi}}^s_2$ do not depend on the design variables. Thus, from the previous expressions it is clear that the products involved in the transformation matrix $\overline{\mathbf{T}}\boldsymbol{\Psi}\mathbf{T}$ are computed once during the design process. Furthermore, due to the structure of the matrices $\overline{\mathbf{T}}$ and $\mathbf{T}$ it can be shown that the previous products involve just permutations of rows and columns of the block diagonal matrices $blockdiag(\overline{\boldsymbol{\Psi}}^1\delta_{10},\ldots,\overline{\boldsymbol{\Psi}}^{N_s}\delta_{N_s0})$, $blockdiag(\overline{\boldsymbol{\Psi}}^1_1\delta_{1j},\ldots,\overline{\boldsymbol{\Psi}}^{N_s}_1\delta_{N_sj})$ and $blockdiag(\overline{\boldsymbol{\Psi}}^1_2\delta_{1j},\ldots,\overline{\boldsymbol{\Psi}}^{N_s}_2\delta_{N_sj})$.

6.5. Final remarks

It is stressed that the efficiency of the above formulation in terms of the number of substructure analyses required is based on the assumption that the substructure matrices depend only on one design variable. For the more general case, the normal and constraint modes have to be recomputed in each iteration of the design process. In fact, when the substructure matrices depend on two or more design variables, a representation similar to Eqs. (24) and (25) is no longer applicable and the reduced substructure matrices of the reduced-order model should be re-assembled from the substructure stiffness and mass matrices for new values of the vector of design variables $\boldsymbol{\theta}$. This repeated computation, however, is usually confined to a small number of substructures in many practical applications. So, even in the more general case a significant saving may still arise since the estimation of the fixed-interface modes and the interface constraint modes for most of the substructures need not to be repeated during the design process. For the general case (dependence on two or more design variables) it is also interesting to note that interpolation schemes can be adopted to avoid re-analyses at the substructure level by approximating the fixed-interface normal modes and the interface constraint modes at various values of the design variables in terms of the corresponding modes of a family of models defined at a number of design points [38]. The use of approximation schemes is, however, outside the scope of the present work. This aspect of the implementation is left for future research efforts (see Conclusions). Finally, it is noted that parallelization techniques are also possible at the model level. In fact, the definition of all substructure matrices in generalized coordinates can be carried out in parallel, reducing the computational time of the proposed implementation even further.

7. Numerical examples

Two numerical examples are presented in this section. The first example, which is considered as a test problem, deals with a simple linear model while the second example, which is considered as an application problem, considers a bridge structure with localized nonlinearities. The objective of the test problem is to evaluate the effectiveness of the proposed model reduction technique in a relatively simple model, while the second example examines the effect of the proposed technique in a more involved model.

7.1. Example 1: test problem

7.1.1. Model description

The structural model shown in Fig. 1 is considered as a test problem. It consists of a three-span two dimensional frame structure. The structure has a total length of 30.0 m and a constant floor height of 5.0 m, leading to a total height of 40.0 m. The finite

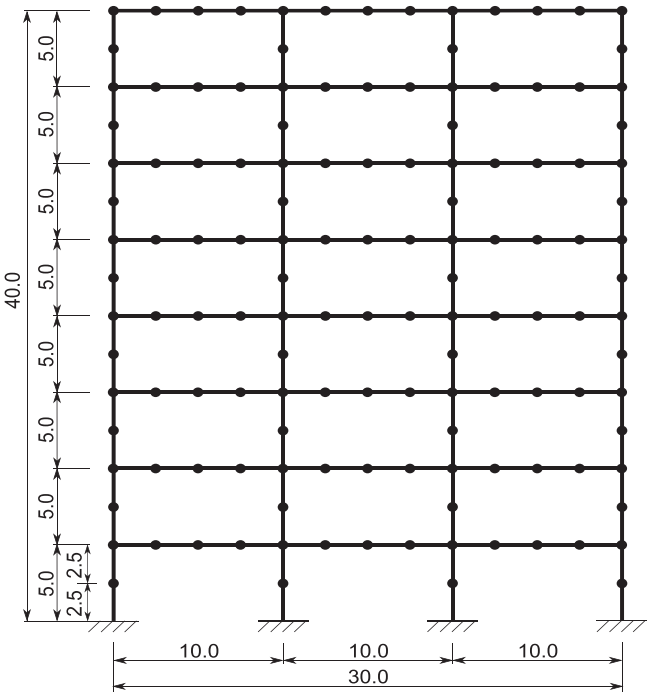

Fig. 1. Three-span eight-story two dimensional frame structure.

element model comprises 160 two dimensional beam elements of square cross section with 140 nodes and a total of 408 degrees of freedom. The dimension of the square cross section of the beam elements is equal to 0.4 m. The axial deformation of the column elements is assumed to be small and they are neglected in the model. Material properties of the beam elements have been assumed as follows: Young's modulus $E=2.0\times10^{10}$ N/m^2, and mass density $\rho=2500$ kg/m^3. A 5% of critical damping for the modal damping ratios is introduced in the model. The structural system is excited horizontally by a ground acceleration modeled as a non-stationary stochastic process. In particular, a stochastic point-source model characterized by a series of seismicity parameters such as the moment magnitude and rupture distance is considered in the present implementation [23,24]. The model is a simple, yet a powerful means for simulating ground motions with high and low frequency components. The methodology, which was initially developed for generating synthetic ground motions, has been reinterpreted to form a stochastic model for ground excitation [39].

The input for the stochastic excitation model involves a white noise sequence and a series of seismological parameters as previously pointed out. Details of the entire procedure can be found in [23,40]. The duration of the excitation is equal to $T=30$ s with a sampling interval equal to $\Delta T=0.01$ s. Based on the characterization of the point source model, the generation of the stochastic ground motions involves more than 3000 random variables for the duration and sampling interval considered. Thus, the vector of uncertain parameters $\mathbf{z}$ involved in the problem (see Section 2) has more than 3000 components. The actual excitation generated for the test problem corresponds to ground motions of low intensity so that the structural response is expected to be dominated by linear elastic behavior, which is compatible with the model under consideration. For illustration purposes, Fig. 2 shows a synthetic excitation sample generated by the stochastic point-source model.

7.1.2. Design problem formulation

The cost C represented by the total volume of the column elements is chosen as the objective function for the design problem. The design variables comprise the dimension of the column elements square cross section of the different floors. In particular, the dimension of the column elements square cross section are linked into two design variables in this example problem. To be more specific, the dimension of the column elements square cross section a is parameterized as $a=\theta\overline{a}$, where $\overline{a}=0.4$ m denotes the nominal dimension and θ is a normalized parameter that represents the design variable. Design variable number one (θ_1) is related to the dimension of the column elements square cross section of floors 1–4, while the second design variable (θ_2) controls the dimension of the column elements square cross section of floors 5–8. To control serviceability, the design criteria are defined in terms of the relative displacements of the first, fifth and eighth floor with respect to the ground. The failure probability functions are defined as

$$P_{F_i}(\boldsymbol{\theta})=P\left[\max_{t\in[0,T]}\frac{|\delta^i(t,\boldsymbol{\theta},\mathbf{z})|}{\delta^{i^*}}>1\right],\quad i=1,2,3 \tag{28}$$

where $\delta^i(t,\boldsymbol{\theta},\mathbf{z})$, $i=1,2,3$ are the relative displacements of the first, fifth and eighth floor with respect to the ground, respectively, and δ^{i^*}, $i=1,2,3$ are the corresponding critical threshold levels. The threshold levels are defined in terms of a percentage of the total height of the frame structure. In particular, the following values are considered: 0.05%; 0.3%; and 0.5% for the threshold levels corresponding to the failure events associated with the first, fifth and eighth floor, respectively. The design problem is formulated as

$$\begin{aligned}&\text{Min}_{\boldsymbol{\theta}}\quad C(\boldsymbol{\theta})\\&\text{s.t.}\quad P_{F_i}(\boldsymbol{\theta})\le10^{-4}\quad i=1,2,3\\&\theta_1\ge\theta_2\\&0.75\le\theta_i\le2.00\quad i=1,2\end{aligned} \tag{29}$$

Note that there are three reliability constraints plus one geometric constraint in addition to the side constraints of the design variables. It is also noted that the estimation of the probability of failure for a given design $\boldsymbol{\theta}$ represents a high-dimensional reliability problem. In fact, as previously indicated, more than three thousands random variables are involved in the corresponding multidimensional probability integral (see Eq. (3)).

7.1.3. Reduced-order model

The structural model is subdivided into sixteen substructures as shown in Fig. 3. Substructures 1–8 are composed by the column elements of the different floors, while substructures 9–16 correspond to the beam elements of the different floors. Based on this subdivision it is noted that substructures 1–4 depend on the design variable θ_1, substructures 5–8 depend on the design variable θ_2, while substructures 9–16 are independent of the design variables. In connection with Section 6, the nonlinear functions of the design variables $\theta_j, j=1,2$ are given by $h^j(\theta_j)=\theta_j^4$ (related to the area second moment of inertia term in the stiffness matrices) and $g^j(\theta_j)=\theta_j^2$ (related to the area term in the mass matrices), respectively.

For each substructure it is selected to retain all fixed-interface normal modes that have frequency ω such that $\omega\le\alpha\omega_c$, with α being a multiplication factor and ω_c is a cut-off frequency which is taken equal to 41.0 rad/s in this case (4th modal frequency of the unreduced reference model). It is noted that the value of the factor α affects the computational efficiency and accuracy of the model reduction technique. The multiplication factor is selected to be 10.0 for substructures 1–8, and 2.9 for substructures 9–16. With this selection of parameters only 1 fixed-interface normal mode is kept for each substructure. Thus, the reduced-order model comprises a total of 16 generalized coordinates out of the 312 internal degrees of freedom of all substructures (95% reduction in terms of the internal degrees of freedom). Note that the total number of interface degrees of freedom is equal to 96 in this case. Table 1 shows the error (in percentage) between the modal frequencies using the unreduced reference finite element model and the modal frequencies computed using the reduced-order model. It is observed that the errors are quite small. In fact, the error for the lowest 4 modes fall bellow 0.1%. The comparison with the lowest 4 modes seems to be reasonable since validation calculations show that the contribution of the higher order modes (higher than the 4th mode) in the dynamic response of the model is negligible.

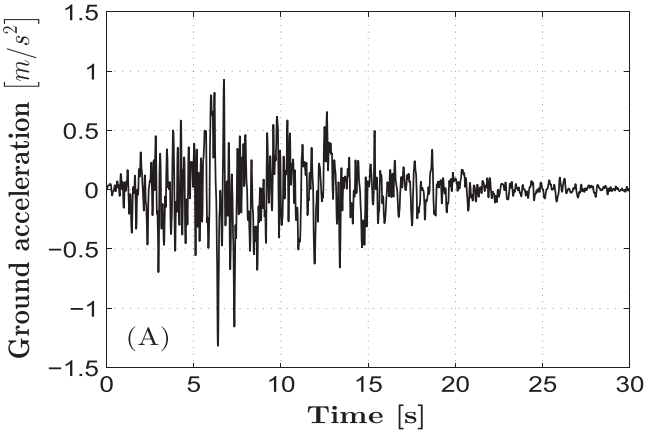

Fig. 2. Excitation time history sample.

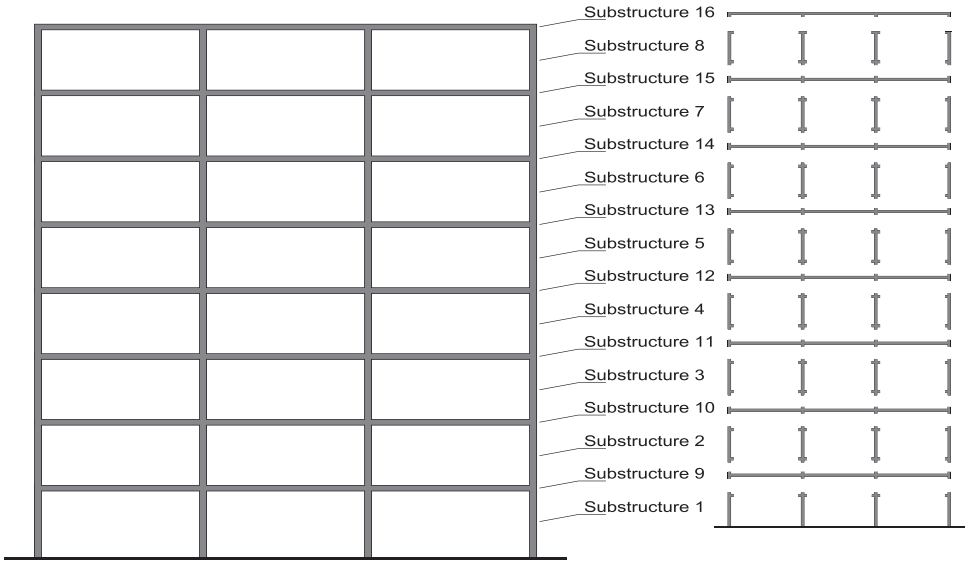

Fig. 3. Substructures of the finite element model for design purposes.

Table 1
Modal frequency error between the modal frequencies of the unreduced reference model and the reduced-order model. Test problem.

Frequency number	Error (%)
1	1.3×10^{-3}
2	1.1×10^{-2}
3	3.4×10^{-2}
4	8.8×10^{-2}

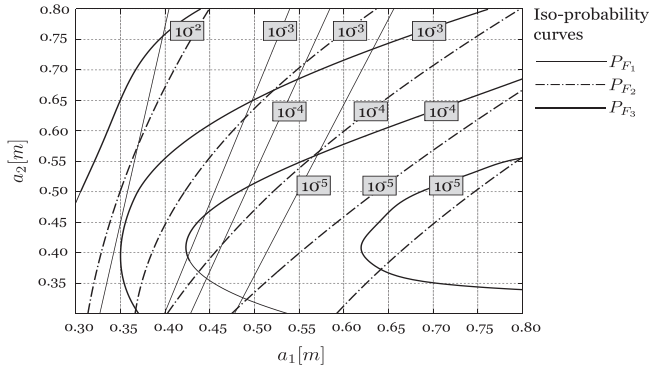

Fig. 4. Iso-probability curves associated with the failure events of the first, fifth, and eighth floor (unreduced model).

It is important to note that the selection of the number of fixed-interface modes per substructure, necessary to achieve a prescribed accuracy, can be done off-line, before the design procedure takes place. This calibration analysis can be carried out not only for the reference model but for other configurations as well. Validation calculations have shown that the reduced-order model is adequate for the entire design space defined in (29). In summary, it is observed that even for this simple model an important reduction in the number of generalized coordinates is obtained with respect to the number of the degrees of freedom of the original unreduced finite element model. In fact, an almost 75% reduction is obtained in this test problem. It is expected that a more significant reduction will be obtained for more involved finite element models (see next example problem).

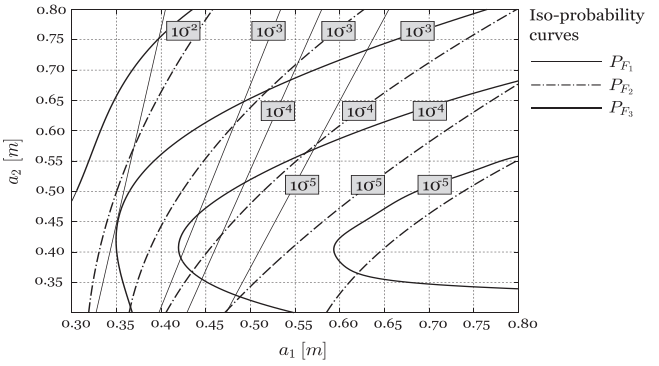

Fig. 5. Iso-probability curves associated with the failure events of the first, fifth, and eighth floor (reduced-order model).

7.1.4. Results

The effectiveness of the model reduction technique in the context of the design problem is investigated in this section. Figs. 4 and 5 show some iso-probability curves in the design space constructed by using the original unreduced model and the reduced-order model, respectively. For clarity, the design space is given directly in terms of the actual dimension of the column elements square cross section. The iso-probability curves correspond to the three failure events defined in Section 7.1.2. These curves are constructed by using a set of failure probability estimates distributed over the design space. Each of the estimate is obtained by subset simulation as indicated before. The resulting curves, which are somewhat rugged because of the variability of the probability estimates, have been smoothed for presentation purposes. It is observed that the iso-probability curves obtained by the full and reduced-order model are almost identical. There is only small differences for some iso-probability curves corresponding to low probability events ($\leq 10^{-5}$), but they follow the same trend. The small differences at low probability levels are due to the simulation scheme used to estimate such probabilities (subset simulation in this case), but they are not due to the performance of the reduced model which is very accurate. The previous result implies that the final design can be obtained with sufficient accuracy by using the reduced-order model instead of the full model.

From the design point of view it is seen that the iso-probability curves associated with the relative displacement of the first floor (P_{F_1}) show a weak interaction between the dimension of the column elements square cross section of the lower and upper floors specially for flexible lower floors columns (i.e. $a_1 \leq 0.4$ m). Under this condition, the iso-probability curves are controlled by the dimension of the column elements square cross section of the lower floors, as expected. For more rigid lower floors columns the interaction between the design variables is somewhat more pronounced. On the other hand, the iso-probability curves related to the relative displacement of the fifth floor (P_{F_2}) show a clear interaction between the dimension of the column elements square cross section of the lower and upper floors. Finally, the iso-probability curves associated with the roof displacement (eighth floor) (P_{F_3}) show a strong non-linear interaction between the dimension of the column elements square cross section of all floors, as anticipated. These results give a valuable insight into the interaction and effect of the design variables on the reliability of the structural model.

Fig. 6 shows the feasible domain, some normalized objective contours and some iso-probability curves as well as the final design. It is observed that the geometric and side constraints are inactive at the final design. The reliability constraints related to the relative displacement of the first and eighth floor with respect to the ground are active at the final design. Starting from the initial feasible design $\theta_1 = 2.0$ ($a_1 = 0.8$ m) and $\theta_2 = 1.625$ ($a_2 = 0.65$ m), the final design is obtained in about ten iterations by using the interior point algorithm described in [33,35] (see Section 4.2). In terms of the computational cost, the number of finite element runs involved during the design process depends on the number of iterations and the number of simulations necessary to estimate the failure probability and its sensitivity for the different designs required by the optimizer. Thus, the computational effort for assembling the finite element model and obtaining its dynamic response for a given design is the key factor for comparison purposes. The results indicate that the speedup achieved by the proposed formulation is about 4, where the speedup is defined as the ratio of the execution time of the design process by using the unreduced original model and the execution time of the design process by using the reduced-order model. As previously pointed out, it is expected that even a more significant reduction in computational cost will be achieved for the cases of more involved models (see next example problem). Finally, it is important to note that this reduction in computational effort is achieved without compromising the accuracy of the final design. In other words, the final design obtained from the reduced-order model is analogous to the one obtained from the unreduced model.

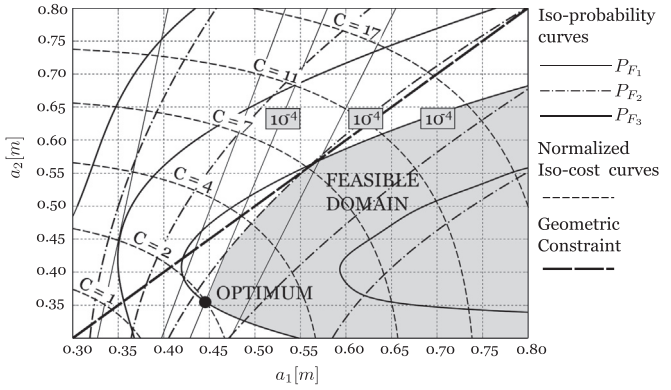

Fig. 6. Feasible domain and optimum design.

7.2. Example 2: Application problem

7.2.1. Structural system

The bridge structural model shown in Fig. 7, which has been borrowed from [18], is used in this section as an application problem. The bridge is curved in plan and has a total length of 119 m. It has 5 spans of lengths equal to 24.0 m, 20.0 m, 23.0 m, 25.0 m, and 27.0 m, respectively, and four piers of 8 m height that support the girder monolithically. Each pier is founded on an array of four piles of 35 m height. The piers and piles are modeled as column elements of circular cross-section with 1.6 m and 0.6 m diameter, respectively. The deck cross section is a box girder which is modeled by beam and shell elements. It rests on each abutment through two rubber bearings that consist of layers of rubber and steel plates, with the rubber being vulcanized to the steel plates. A schematic representation of a rubber bearing is also shown in the figure, where D_r represents the external diameter, D_i=0.1 m is the internal diameter, and $H_r = n_r t_r$ is the total height of rubber in the bearing, where t_r is the layer thickness and n_r is the number of rubber bearings. The force-displacement characteristics of the rubber bearings are modeled by a biaxial hysteretic behavior. An analytical model based on a series of experimental tests conducted for real-sized rubber bearings is used in the present application. For a detailed description of the analytical model that describe the nonlinear behavior of the bearings the reader is referred to [41]. The interaction between the piles and the soil is modeled by a series of translational springs along the height of the piles with stiffnesses varying from 11,200 T/m at the base to 0.0 T/m at the surface.

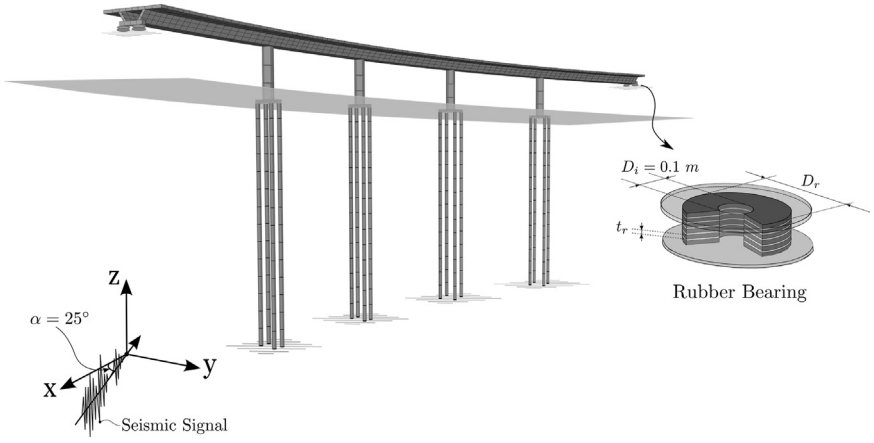

Fig. 7. Finite element model of bridge structure.

Table 2
Nominal values of structural parameters.

Structural parameter	Nominal value (m)
$\overline{D}_{pi}, i=1,2,3,4$	1.6
$\overline{D}_{Lr}$	0.8
$\overline{H}_{Lr}$	0.17
$\overline{D}_{Rr}$	0.8
$\overline{H}_{Rr}$	0.17

The net effect of these elements is to increase the translational stiffness in the x and y direction of the column elements that model the piles. The following values of the material properties of the concrete structure are considered. The Young's modulus is taken to be $E=2.0\times10^{10}$ N/m^2, the Poisson ratio $\nu=0.2$, and mass density $\rho=2500$ kg/m^3. Finally, a 3% of critical damping is added to the model. The selected finite element model for the bridge structure has 10,068 degrees of freedom. In what follows, it is assumed that the previous model is representative of the actual behavior of the bridge structure and it is referred to as the nominal model. In this context, it is assumed that the structural components such as the piers, piles and the deck girder remain linear during the analysis while the nonlinearities are localized in the rubber bearings response. In addition, the axial deformation of the piers is neglected with respect to their bending deformation. The bridge structure is subjected to a ground acceleration in a direction defined at 25° with respect to the x-axis as shown in Fig. 7. Such ground acceleration is modeled as in the previous example, that is, by a stochastic point-source model. The duration of the excitation is equal to $T=20$ s with a sampling interval equal to $\Delta T=0.01$ s. In this case, the generation of the stochastic ground motions comprise more than 2000 random variables and therefore the vector of uncertain parameters $\mathbf{z}$ involved in the problem has more than 2000 components.

7.2.2. Reliability-based design formulation

The reliability-based design problem is defined in terms of the following constrained non-linear optimization problem

$$\begin{aligned}&\text{Min}_{\boldsymbol{\theta}} \quad C(\boldsymbol{\theta})\\ &\quad P_{F_i}(\boldsymbol{\theta}) \le P^*_{F_i}, \quad i=1,2\\ &\quad \boldsymbol{\theta}\in\Theta\end{aligned} \tag{30}$$

where $\boldsymbol{\theta},\theta_i,\ i=1,\ldots,8$ is the vector of design variables, $C(\boldsymbol{\theta})$ is the objective function, $P_{F_i}(\boldsymbol{\theta}),\ i=1,2$ are the failure probability functions, and $P^*_{F_i}, i=1,2$ are the corresponding target failure probabilities which are taken equal to $P^*_{F_i}=10^{-4}, i=1,2$. The design variables include the diameter of the piers circular cross section, and the external diameter and total height of rubber in the bearings. Design variables $\theta_1,\theta_2,\theta_3$ and θ_4 are related to the diameter of the circular cross section of the four piers, while design variables $\theta_5,\theta_6,\theta_7$ and θ_8 are associated with the external diameter and the total height of rubber of the bearings located at the abutments. The relationship between the design variables and the actual structural parameters is given by $D_{pi}=\theta_i\overline{D}_{pi},\ i=1,2,3,4$, $D_{Lr}=\theta_5\overline{D}_{Lr}$, $H_{Lr}=\theta_6\overline{H}_{Lr}$, $D_{Rr}=\theta_7\overline{D}_{Rr}$, and $H_{Rr}=\theta_8\overline{H}_{Rr}$, where D_{pi}, $i=1,2,3,4$ are the diameters of the circular cross section of the piers, D_{Lr} and D_{Rr} are the external diameters of the bearings located at the left and right abutments, respectively, H_{Lr} and H_{Rr} are the total heights of rubber of the bearings located at the left and right abutments, respectively, and $\overline{D}_{pi}$, $\overline{D}_{Lr}$, $\overline{H}_{Lr}$, $\overline{D}_{Rr}$, $\overline{H}_{Rr}$ are the corresponding nominal values of the parameters which are given in Table 2.

The side constraints for the design variables are given by: $0.75\le\theta_i\le1.25,\ i=1,2,3,4;\quad 0.75\le\theta_i\le1.25,\ i=5,7,$ and $0.88\le\theta_i\le1.47, i=6,8$. The objective function $C(\boldsymbol{\theta})$ represents a cost function which is assumed to be proportional to the total volume of rubber in the bearings and to the total volume of the piers. Failure, that is unacceptable performance, is defined in terms of the relative displacement of piers and the relative displacement of the rubber bearings. Thus, the corresponding failure probability functions are given by

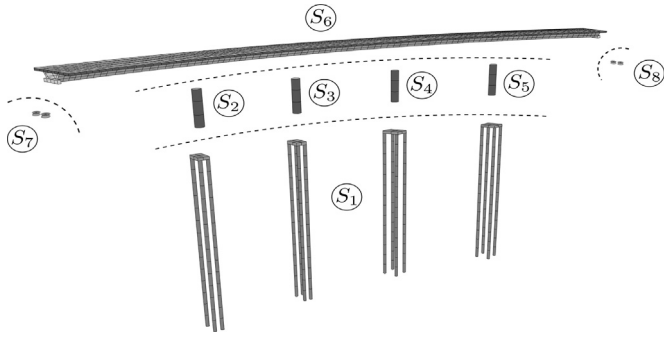

Fig. 8. Substructures of the finite element model used for design purposes.

$$\begin{aligned}P_{F_1}(\boldsymbol{\theta}) &= P\left[\max_{t\in[0,T]}\frac{|u_{b\max}(t,\boldsymbol{\theta},\mathbf{z})|}{0.10\text{ m}}>1\right],\\ P_{F_2}(\boldsymbol{\theta}) &= P\left[\max_{t\in[0,T]}\frac{|\delta_{\max}(t,\boldsymbol{\theta},\mathbf{z})|}{0.07\text{ m}}>1\right]\end{aligned} \tag{31}$$

where $u_{b\max}(t,\boldsymbol{\theta},\mathbf{z})$ represents the maximum relative displacement between the deck girder and the base of the rubber bearings at each abutment (in the x or y direction), and $\delta_{\max}(t,\boldsymbol{\theta},\mathbf{z})$ denotes the maximum relative displacement between the top of the piers and their connection with the piles foundations (in the x or y direction). Note that the estimation of the failure probability functions for a given design $\boldsymbol{\theta}$ represents a high-dimensional reliability problem as in the test problem.

7.2.3. Substructures characterization

Considering the previous design formulation the bridge structure is divided into a number of substructures. The division is guided by a parametrization scheme so that the substructure matrices for each one of the introduced substructures depend on only one of the design variables. In particular, the structural model is subdivided into six linear substructures and two nonlinear substructure as shown in Fig. 8. Substructure S_1 is composed by the pile elements, substructures S_2, S_3, S_4 and S_5 include the different pier elements, and substructure S_6 corresponds to the deck girder. Finally, substructures S_7 and S_8 are the nonlinear substructures composed by the rubber bearings located at the left and right abutment, respectively. With this subdivision substructures S_1 and S_6 do not depend on the design variables, while substructures S_2, S_3, S_4 and S_5 depend on the design variables θ_1, θ_2, θ_3, and θ_4, respectively, and design variables θ_5, θ_6, θ_7, and θ_8 are associated with the nonlinear substructures S_7 and S_8. The nonlinear functions of the design variables $\theta_j, j=1,2,3,4$ corresponding to the linear substructures are given by $h^j(\theta_j)=\theta_j^4$, and $g^j(\theta_j)=\theta_j^2$, respectively.

Based on an analysis similar to the one performed in the previous example problem it is concluded that retaining ten generalized coordinates for substructure S_1, two for each one of substructures S_2, S_3, S_4 and S_5, and ten for substructure S_6 is adequate in the context of this application. The error (in percentage) between the modal frequencies using the full nominal reference finite element model and the modal frequencies computed using the reduced-order model is shown in Table 3. The modal frequencies for both models are computed by considering only the linear components of the structural system. It is seen that with this number of generalized coordinates the error fall bellow 0.5% for the lowest

Table 3
Modal frequency error between the modal frequencies of the full model and the reduced-order model.

Frequency number	Unreduced model	Reduced-order model	Error
	ω (rad/s)	ω (rad/s)	(%)
1	4.214	4.216	0.05
2	4.282	4.284	0.06
3	4.569	4.572	0.06
4	12.197	12.249	0.43
5	15.424	15.462	0.25
6	23.419	23.421	0.01

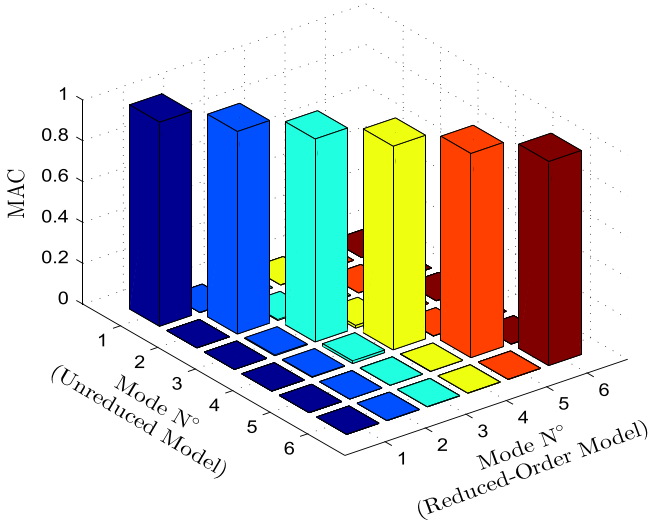

Fig. 9. MAC-values between the mode shapes computed from the unreduced finite element model and from the reduced-order model.

6 modes. The corresponding matrix of MAC-values (modal assurance criterion) between the first six modal vectors computed from the unreduced finite element model and from the reduced-order model is shown in terms of a 3-D representation in Fig. 9. It is observed that the values at the diagonal terms are close to one and almost zero at the off-diagonal terms. Thus, the modal vectors of both models are consistent. The comparison with the lowest 6 modes is based on the fact that the contribution of the higher order modes (higher than the 6th mode) in the dynamic response of the model is negligible. In summary, a total of 28 generalized coordinates, corresponding to the fixed interface normal modes of the linear substructures, out of 10,008 internal DOF of the original model, are retained for the six linear substructures. On the other hand, the number of interface degrees of freedom is equal to 60 in this case. With this reduction, the total number of generalized coordinates of the reduced-order model represents a 99% reduction with respect to the unreduced model. Thus, a drastic reduction in the number of generalized coordinates is obtained with respect to the number of the degrees of freedom of the original unreduced finite element model. Based on the previous analysis, it is concluded that the reduced-order model and the full unreduced model are equivalent in the context of this application problem. Therefore, the design process of the bridge structural model is carried out by using the reduced-order model. As previously pointed out the calibration of the reduced-order model can be done off-line, before the design procedure takes place.

7.2.4. Design results

Taking advantage of the reduced-order model a couple of design scenarios are investigated in detail in order to get insight

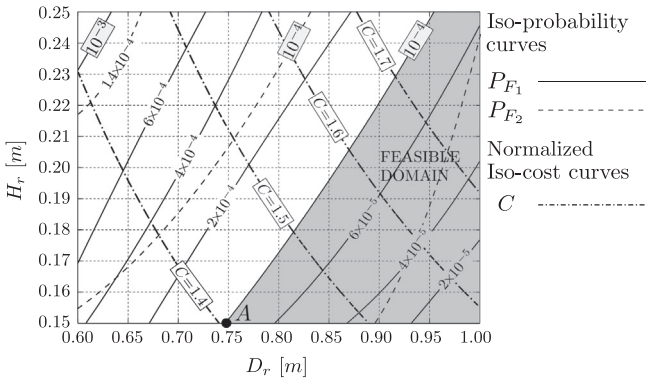

Fig. 10. Design space in terms of the design variables associated with the rubber bearings (D_r, H_r). P_{F_1}: iso-probability curves of failure event F_1. P_{F_2}: iso-probability curves of failure event F_2. C: normalized objective function contours.

into the reliability and general performance of the bridge structure under consideration. First, the design of the rubber bearings (isolators) located at the abutments is considered. In particular, the effect of the external diameter and the total height of rubber in the bearings on the design of such elements is studied. To this end, the design variables θ_1, θ_2, θ_3, and θ_4, which control the diameters of the circular cross sections of the piers, are kept constant and equal to their upper bound values $\theta_i = 1.25, i = 1, 2, 3, 4$ ($D_{pi} = 2.0$ m). This is done in order to isolate the effect of the design variables associated with the rubber bearings. Moreover, these variables are linked into two design variables, one related to the external diameter ($\theta_{D_r} = \theta_5 = \theta_7$) and the other related to the total height of rubber ($\theta_{H_r} = \theta_6 = \theta_8$). In other words all rubber bearings are assumed to have the same geometrical properties. With the previous setting Fig. 10 shows some iso-probability curves and objective function contours as well as the final design.

The design space is shown in terms of the actual values of the external diameter ($D_r = \theta_{D_r}\overline{D}_r$) and the total height of rubber ($H_r = \theta_{H_r}\overline{H}_r$). The objective contours are normalized by a cost factor and the iso-probability curves are constructed by using a set of failure estimates distributed over the design space. As in the previous example these curves have been smoothed for presentation purposes. It is important to note that these curves were constructed by the reduced-order model in a reasonable computational time. The construction of these curves from the full finite element model is not practical due to the excessive computational time required to estimate the failure probabilities over the design space. From the figure it is seen that the probability of the failure event F_1 decreases as the external diameter of the isolators increases. This is reasonable since the isolation system becomes stiffer with rubber bearings having larger external diameters and thus the relative displacements between the deck girder and the base of the rubber bearings at each abutment, which control the failure event F_1, are expected to decrease. On the contrary, the failure probability increases as the height of rubber increases. In this case the isolation system becomes more flexible and therefore the relative displacements between the deck girder and the base of the rubber bearings increase. A similar effect is observed with respect to the failure event related to the relative displacement between the top of the piers and their connection with the piles foundations (F_2). That is, an increase of the external diameter of the isolators decreases the probability of failure event F_2 since the overall system becomes stiffer. On the other hand, an increase of the total height of rubber in the isolators increases the probability of failure event F_2 since in this case the structural system becomes more flexible. The corresponding final design is given by D_r=0.75 m and H_r=0.15 m. The side constraint associated with the height of rubber and the reliability constraint related to the

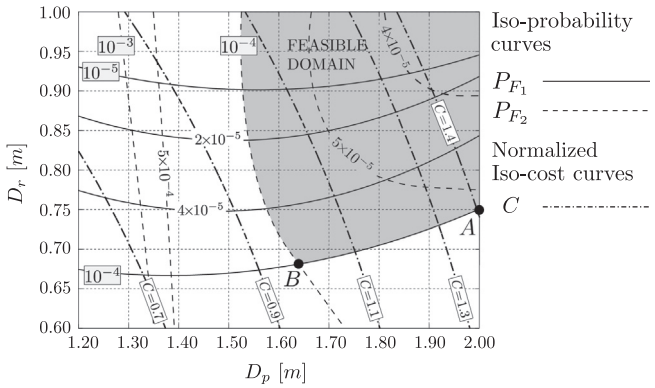

Fig. 11. Design space in terms of the diameter of the circular cross sections of the piers (D_p) and the external diameter of the rubber bearings (D_r). P_{F_1}: iso-probability curves of failure event F_1. P_{F_2}: iso-probability curves of failure event F_2. C: normalized objective function contours.

maximum relative displacement between the deck girder and the base of the rubber bearings at each abutment are active at the final design. Contrarily, the reliability constraint associated with the maximum relative displacement between the top of the piers and their connection with the piles foundations is inactive.

Next, the interaction between bridge structural components and rubber bearing parameters is considered. Specifically, the design space in terms of the diameter of the circular cross sections of the piers and the external diameter of the rubber bearings is constructed. For this purpose the design variables associated with the diameters of the circular cross sections of the piers are linked to one design variable $\theta_{D_{\text{pier}}}$, i.e. $\theta_{D_{\text{pier}}}=\theta_1=\theta_2=\theta_3=\theta_4$, while the design variables θ_5 and θ_7 associated with the external diameters of the rubber bearings are linked to one design variable θ_{D_r}, i.e, $(\theta_{D_r}=\theta_5=\theta_7)$. Design variables related to the total heights of rubber in the bearings are kept constants and equal to their lower bound values, i.e, $\theta_6=\theta_8=0.88$ (H_r=0.15 m). Fig. 11 shows some objective contours and iso-probability curves as well as the final design. As in the previous figure, the design space is shown in terms of the actual values of the diameter of the circular cross sections of the piers ($D_p=\theta_{D_{\text{pier}}}\overline{D}_p$) and the external diameter of the rubber bearings ($D_r=\theta_{D_r}\overline{D}_r$). From the figure it is observed that the probability of failure event F_2 decreases as the diameter of the circular cross sections of the piers increase. In this case the piers become stiffer and therefore the relative displacements between the top of the piers and their connection with the piles foundations decrease. It is also seen that the failure event F_2 is controlled by the diameter of the circular cross sections of the piers for values of this quantity close to its lower bound, i.e. $D_p\leq 1.45$ m. In this range of values the iso-probability curves are almost perpendicular. So, the effect of the external diameter of the isolator is negligible. In other words, the flexibility of the pier elements controls the relative displacements between the top of the piers and their connection with the piles foundations, as expected. Contrarily, for values of this quantity close to its upper bound, i.e. $D_p\geq 1.70$ m a strong interaction between the diameter of the circular cross sections of the piers and the external diameter of the rubber bearings is observed. Thus, for rigid pier elements the relative displacements between the top of the piers and their connection with the piles foundations is controlled by both design variables, that is, D_p and D_r. In fact, the iso-probability curves indicate that for example an increase in the diameter of the circular cross sections of the piers is compensated by a decrease in the external diameter of the bearings. In other words, for such combination of the design variables D_p and D_r the probability of failure remains invariant. On the other hand it seen that the failure event F_1 is mainly controlled by the external diameter of the rubber bearings. Actually, the iso-probability curves associated with failure event F_1 show a relatively weak interaction between the diameter of the circular cross sections of the piers and the external diameter of the rubber bearings. The probability of failure of this event decreases as the external diameter of the isolators increases, which is the same behavior observed in Fig. 10. The final design for this scenario is given by D_p=1.64 m and D_r=0.67 m (point B in the figure) where both reliability constraints are active.

The results shown in Fig. 11 can also be used to demonstrate the benefits of designing the isolators and the bridge structure simultaneously. For example, if the design process involves only the isolators and the diameter of the circular cross sections of the piers are kept constant at their upper bound values (D_p=2.0 m), the optimal design is given by D_r=0.75 m (point A in the figure) with a corresponding normalized cost equal to C=1.4. On the other hand, if the diameter of the circular cross sections of the piers is also considered as design variable the final design moves from point A to point B, with a decrease of the normalized cost in about 30%. Thus, taking into account the interaction between the design variables associated with the bridge structure and the isolators during the design process is quite beneficial in terms of the cost of the final design. It is interesting to note that the final design previously obtained can be improved just marginally if the eight design variables are considered as independent during the design process. It can be shown that in this case the nominal cost is decreased in about 5% with respect the final design shown in Fig. 11. The corresponding design process converges in less than fifteen iterations starting from the initial feasible design given by $D_{pi}=2.0$ m, $i=1,2,3,4$, $D_{Lr}=D_{Rr}=1.0$ m and $H_{Lr}=H_{Rr}=0.25$ m.

Finally, it is noted that the above observations and remarks give a valuable insight into the complex interaction of the design variables on the performance and reliability of the bridge structural system.

Table 4
On-line computational cost of different tasks for a given design.

Task	Full finite element model	Reduced-order model	
	Time (s)	Time (s)	Speedup
Finite element generation	52.9	0.013	4069
Modal analysis	0.74	0.052	14
Dynamic response	1.7	0.51	3
Sum of different tasks	55.34	0.58	95

7.2.5. Computational cost

Table 4 shows the on-line computational costs involved in the assemblage of the finite element model and the computation of the dynamic response for a given design considering the full finite element model and the reduced-order model. These operations and procedures are performed at each iteration of the design process. The last column of the table indicates the speedup (round to the nearest integer) achieved by the reduced-order model for the different tasks. As previously pointed out, the speedup is the ratio of the execution time by using the unreduced model and the execution time by using the reduced-order model. It is seen that the difference is quite significant. In fact, the overall speedup for the online calculations is more than 90 in this case (last row of the table).

The off-line computational cost, that is the cost of calculations related to the definition of the reduced-order model and the characterization of the transformation matrix that maps the generalized coordinates to the physical coordinates of the unreduced model, which are preformed once during the design process, corresponds to approximately two full analyses (finite element

model generation and dynamic response) of the unreduced model in this case. Considering this cost an overall speedup value of about 10 is obtained by the proposed methodology in solving this particular design problem. However, once the reduced-order model has been defined several design scenarios, i.e. in terms of different objective functions and reliability constraints, can be explored and solved efficiently. So, high speedup values (20, 40 or even more) can be obtained for the design process as a whole. As previously pointed out this reduction in computational effort is achieved without compromising the accuracy of the final design.

8. Conclusions

A general strategy for dealing with a class of reliability-based design problems of stochastic finite elements has been presented. It consists in the integration of a model reduction technique with an appropriate optimization scheme. The design process is carried out in a reduced space of generalized coordinates. In particular, a model reduction technique based on fixed interface normal modes and interface constraint modes is considered in the present implementation. The reduction technique, which is applied to the linear components of the structural systems, produces highly accurate models with relatively few substructure modes. Numerical examples indicate that the integration of the proposed model reduction technique in the framework of reliability-based optimization is applicable for a class of linear and nonlinear finite element models under stochastic excitation. The results also demonstrate that the computational effort involved during the design process is reduced significantly with respect to the process considering the unreduced finite element model. In fact, good speedup values were obtained. On the other hand, the reduction in computational effort is achieved without compromising the accuracy of the design process. Based on the results of this study it is concluded that the proposed approach is potentially an effective tool for solving a class of reliability-based design problems involving complex structural systems under stochastic excitation. Future research directions aim at considering more involved problems from the optimization point of view (formulations with more design variables) as well as the implementation of design process in a fully parallel environment. In addition, the implementation of interpolation schemes for approximating fixed-interface normal modes and interface constraint modes for cases in which the substructure matrices depend on more than one design variable is another research effort. Work in these directions are currently under consideration.

Acknowledgments

The research reported here was supported in part by CONICYT under grant number 1150009 which is gratefully acknowledged by the authors. Also this research has been implemented under the "ARISTEIA" Action of the "Operational Programme Education and Lifelong Learning" and was co-funded by the European Social Fund (ESF) and Greek National Resources.

Appendix A

The matrices $\hat{\mathbf{K}}_0$, $\hat{\bar{\mathbf{K}}}_{1j}$ and $\hat{\bar{\mathbf{K}}}_{2j}, j=1,\ldots,n_d$ are defined as

$$\hat{\mathbf{K}}_0 = \mathbf{T}^T \begin{bmatrix} \hat{\mathbf{K}}_0^1 \delta_{10} & \mathbf{0} & \mathbf{0} \\ \mathbf{0} & \ddots & \mathbf{0} \\ \mathbf{0} & \mathbf{0} & \hat{\mathbf{K}}_0^{N_s} \delta_{N_s 0} \end{bmatrix} \mathbf{T},$$

$$\hat{\bar{\mathbf{K}}}_{1j} = \mathbf{T}^T \begin{bmatrix} \hat{\bar{\mathbf{K}}}_1^1 \delta_{1j} & \mathbf{0} & \mathbf{0} \\ \mathbf{0} & \ddots & \mathbf{0} \\ \mathbf{0} & \mathbf{0} & \hat{\bar{\mathbf{K}}}_1^{N_s} \delta_{N_s j} \end{bmatrix} \mathbf{T}$$

$$\hat{\bar{\mathbf{K}}}_{2j} = \mathbf{T}^T \begin{bmatrix} \hat{\bar{\mathbf{K}}}_2^1 \delta_{1j} & \mathbf{0} & \mathbf{0} \\ \mathbf{0} & \ddots & \mathbf{0} \\ \mathbf{0} & \mathbf{0} & \hat{\bar{\mathbf{K}}}_2^{N_s} \delta_{N_s j} \end{bmatrix} \mathbf{T} \tag{32}$$

where $\hat{\mathbf{K}}_0^s$ represents the stiffness matrix in generalized coordinates $\mathbf{v}^s(t)$ of a substructure that does not depend on the design variables, i.e. $\delta_{s0}=1$ if $s \in S_0$, and $\delta_{s0}=0$ otherwise, and

$$\hat{\bar{\mathbf{K}}}_1^s = \begin{bmatrix} \overline{\mathbf{\Lambda}}_{kk}^s & \mathbf{0}_{kb}^s \\ \mathbf{0}_{bk}^s & \mathbf{0}_{bb}^s \end{bmatrix}, \quad \hat{\bar{\mathbf{K}}}_2^s = \begin{bmatrix} \mathbf{0}_{kk}^s & \mathbf{0}_{kb}^s \\ \mathbf{0}_{bk}^s & \overline{\mathbf{K}}_{bb}^s + \overline{\mathbf{K}}_{bi}^s \overline{\mathbf{\Psi}}_{ib}^s \end{bmatrix} \tag{33}$$

where $\delta_{sj}=1$ if $s \in S_j$ and $\delta_{sj}=0$ otherwise. On the other hand, the matrices $\hat{\mathbf{M}}_0$, $\hat{\bar{\mathbf{M}}}_{1j}$, $\hat{\bar{\mathbf{M}}}_{2j}$, and $\hat{\bar{\mathbf{M}}}_{3j}, j=1,\ldots,n_d$ are given by

$$\hat{\mathbf{M}}_0 = \mathbf{T}^T \begin{bmatrix} \hat{\mathbf{M}}_0^1 \delta_{10} & \mathbf{0} & \mathbf{0} \\ \mathbf{0} & \ddots & \mathbf{0} \\ \mathbf{0} & \mathbf{0} & \hat{\mathbf{M}}_0^{N_s} \delta_{N_s 0} \end{bmatrix} \mathbf{T},$$

$$\hat{\bar{\mathbf{M}}}_{1j} = \mathbf{T}^T \begin{bmatrix} \hat{\bar{\mathbf{M}}}_1^1 \delta_{1j} & \mathbf{0} & \mathbf{0} \\ \mathbf{0} & \ddots & \mathbf{0} \\ \mathbf{0} & \mathbf{0} & \hat{\bar{\mathbf{M}}}_1^{N_s} \delta_{N_s j} \end{bmatrix} \mathbf{T}$$

$$\hat{\bar{\mathbf{M}}}_{2j} = \mathbf{T}^T \begin{bmatrix} \hat{\bar{\mathbf{M}}}_2^1 \delta_{1j} & \mathbf{0} & \mathbf{0} \\ \mathbf{0} & \ddots & \mathbf{0} \\ \mathbf{0} & \mathbf{0} & \hat{\bar{\mathbf{M}}}_2^{N_s} \delta_{N_s j} \end{bmatrix} \mathbf{T},$$

$$\hat{\bar{\mathbf{M}}}_{3j} = \mathbf{T}^T \begin{bmatrix} \hat{\bar{\mathbf{M}}}_3^1 \delta_{1j} & \mathbf{0} & \mathbf{0} \\ \mathbf{0} & \ddots & \mathbf{0} \\ \mathbf{0} & \mathbf{0} & \hat{\bar{\mathbf{M}}}_3^{N_s} \delta_{N_s j} \end{bmatrix} \mathbf{T} \tag{34}$$

where $\hat{\mathbf{M}}_0^s$ represent the mass matrix in generalized coordinates $\mathbf{v}^s(t)$ of a substructure that does not depend on the design variables, and

$$\hat{\bar{\mathbf{M}}}_1^s = \begin{bmatrix} \mathbf{I}_{kk} & \mathbf{0}_{kb}^s \\ \mathbf{0}_{bk}^s & \mathbf{0}_{bb}^s \end{bmatrix},$$

$$\hat{\bar{\mathbf{M}}}_2^s = \begin{bmatrix} \mathbf{0}_{kk}^s & \overline{\mathbf{\Phi}}_{ik}^{sT} \overline{\mathbf{M}}_{ii}^s \overline{\mathbf{\Psi}}_{ib}^s + \overline{\mathbf{\Phi}}_{ik}^{sT} \overline{\mathbf{M}}_{ib}^s \\ (\overline{\mathbf{\Phi}}_{ik}^{sT} \overline{\mathbf{M}}_{ii}^s \overline{\mathbf{\Psi}}_{ib}^s + \overline{\mathbf{\Phi}}_{ik}^{sT} \overline{\mathbf{M}}_{ib}^s)^T & \mathbf{0}_{bb}^s \end{bmatrix}$$

$$\hat{\bar{\mathbf{M}}}_3^s = \begin{bmatrix} \mathbf{0}_{kk}^s & \mathbf{0}_{kb}^s \\ \mathbf{0}_{bk}^s & (\overline{\mathbf{\Psi}}_{ib}^{sT} \overline{\mathbf{M}}_{ii}^s + \overline{\mathbf{M}}_{bi}^s) \overline{\mathbf{\Psi}}_{ib}^s + \overline{\mathbf{\Psi}}_{ib}^{sT} \overline{\mathbf{M}}_{ib}^s + \overline{\mathbf{M}}_{bb}^s \end{bmatrix} \tag{35}$$

where all terms have been previously defined.

References

[1] Haftka RT, Gürdal Z. Elements of structural optimization. 3rd edition. New York: Kluwer; 1992.
[2] Enevoldsen I, Sørensen JD. Reliability-based optimization in structural engineering. Struct Saf 1994;15(3):169–96.
[3] Kuschel N, Rackwitz R. Two basic problems in reliability-based structural optimization. Math Methods Oper Res 1997;46(3):309–33.
[4] Royset JO, Der Kiureghian A, Polak E. Reliability-based optimal structural design by the decoupling approach. Reliab Eng Syst Saf 2001;73(3):213–21.
[5] Soong T, Grigoriu M. Random vibration of mechanical and structural systems. Englewood Cliffs, NJ: Prentice Hall; 1993.
[6] Bathe KJ. Finite element procedures. New Jersey: Prentice Hall; 2006.
[7] Au SK, Beck JL. Estimation of small failure probabilities in high dimensions by subset simulation. Probab Eng Mech 2001;16(4):263–77.

[8] Koutsourelakis PS, Pradlwarter HJ, Schuëller GI. Reliability of structures in high dimensions, part I: algorithms and applications. Probab Eng Mech 2004;19(4):409–17.
[9] Schuëller GI, Pradlwarter HJ, Koutsourelakis PS. A critical appraisal of reliability estimation procedures for high dimensions. Probab Eng Mech 2004;19(4):463–74.
[10] Papadrakakis M, Lagaros ND. Reliability-based structural optimization using neural networks and Monte Carlo simulation. Comput Methods Appl Mech Eng 2002;191:3491–507.
[11] Jensen HA, Valdebenito MA, Schuëller GI, Kusanovic DS. Reliability-based optimization of stochastic systems using line search. Comput Methods Appl Mech Eng 2009;198(49–52):3915–24.
[12] Taflanidis AA, Beck JL. Stochastic subset optimization for optimal reliability problems. Probab Eng Mech 2008;23(2–3):324–38.
[13] Schuëller GI, Jensen HA. Computational methods in optimization considering uncertainties - an overview. Comput Methods Appl Mech Eng 2008;198(1):2–13.
[14] Wang J, Katafygiotis LS. Reliability-based optimal design of linear structures subject to stochastic excitations. Struct Saf 2014;47:29–38.
[15] Craig Jr. RR. Structural dynamics, an introduction to computer methods. New York: John Wiley & Sons; 1981.
[16] Hinke L, Dohnal F, Mace B, Waters T, Ferguson. N. Component mode synthesis as a framework for uncertainty analysis. J Sound Vib 2009;324(1–2):161–78.
[17] Papadimitriou C, Papadioti DCh. Component mode synthesis techniques for finite element model updating. Comput Struct 2013;126:15–28.
[18] Jensen HA, Mayorga F, Papadimitriou C. Reliability sensitivity analysis of stochastic finite element models. Comput Methods Appl Mech Eng 296, 2015, 327-351.
[19] Jensen HA, Millas E, Kusanovic D, Papadimitriou C. Model-reduction techniques for Bayesian finite element model updating using dynamic response data. Comput Methods Appl Mech Eng 2014;279:301–24.
[20] Baber TT, Wen Y. Random vibration hysteretic, degrading systems. J Eng Mech Div 1981;107(6):1069–87.
[21] Park YJ, Wen YK, Ang AH. Random vibration of hysteretic systems under bi-directional ground motions. Earthquake Eng Struct Dyn 1986;14(4):543–57.
[22] Lutes L, Sarkani S. Random vibrations, analysis of structural and mechanical systems. Oxford, UK: Elsevier; 2004.
[23] Boore DM. Simulation of ground motion using the stochastic method. Pure Appl Geophys 2003;160(3–4):635–76.
[24] Atkinson GM, Silva W. Stochastic modeling of California ground motions. Bull Seismol Soc Am 2000;90(2):255–74.
[25] Taflanidis A, Jia G. A simulation -based framework for risk assessment and probabilistic sensitivity analysis of base-isolated structures. Earthq Eng Struct Dyn 2011;40:1629–51.
[26] Fishman GS. Monte Carlo: concepts, algorithms and applications. New York, NY: Springer; 1996.
[27] Metropolis N, Ulam S. The Monte Carlo method. J Am Stat Assoc 1949;44(247):335–41.
[28] Ching J, Au SK, Beck JL. Reliability estimation for dynamical systems subject to stochastic excitation using subset simulation with splitting. Comput Methods Appl Mech Eng 2005;194(12–16):1557–79.
[29] Zuev KM, Beck JL, Au SK, Katafygiotis L. Bayesian post-processor and other enhancements of subset simulation for estimating failure probabilities in high dimensions. Comput Struct 2012;92–93:283–96.
[30] Angelikopoulos P, Papadimitriou C, Koumoutsakos P. Bayesian uncertainty quantification and propagation in molecular dynamics simulations: A high performance computing framework. J Chem Phys 2012;137(14).
[31] Au S-K, Wang Y. Engineering risk assessment with subset simulation. John Wiley & Sons; 2014.
[32] Spall JC. Introduction to stochastic search and optimization, estimation, simulation and control. Hobeken, New Jersey: Wiley; 2003.
[33] Herskovits J, Santos G. On the computer implementation of feasible direction interior point algorithms for nonlinear optimization. Struct Optim 1997;14(2–3):165–72.
[34] Baronand FJ, Pironneau O. Multidisciplinary optimal design of a wing profile. In: Proceedings of structural optimization 93. COPPE, Rio de Janeiro, Brazil. 1993. p. 61–8.
[35] Jensen HA, Becerra L, Valdebenito M. On the use of a class of interior point algorithms in stochastic structural optimization. Comput Struct 2013;126:69–85.
[36] Tisseur F, Meerbergen K. The quadratic eigenvalue problem. SIAM Rev 2001;34(2):235–86.
[37] Ma F, Morzfeld M. A general methodology for decoupling damped linear systems. Proc Eng 2011;314:2498–502.
[38] Goller B, Pradlwarter H, Schueller GI. An interpolation scheme for the approximation of dynamical systems. Comput Methods Appl Mech Eng 2011;200:414–23.
[39] Au SK. Reliability-based design sensitivity by efficient simulation. Comput Struct 2005;83(14):1048–61.
[40] Mavroeidis GP, Papageorgiou AS. A mathematical representation of near-fault ground motions. Bull Seismol Soc Am 2003;93(3):1099–131.
[41] Yamamoto M, Minewaki S, Yoneda H, Higashino M. Nonlinear behavior of high-damping rubber bearings under horizontal bidirectional loading: full-scale test and analytical modeling. Earthq Eng Struct Dyn 2012;41(13):1845–60.